Journal of Advances in Modeling Earth Systems

RESEARCH ARTICLE
10.1029/2018MS001299

Application of Discrete Element Methods to Approximate Sea Ice Dynamics

A. Damsgaard[1], A. Adcroft[1], and O. Sergienko[1]

[1]Program in Atmospheric and Oceanic Sciences, Princeton University, Princeton, NJ, USA

Key Points:
- Abrupt strengthening under dense ice-packing configurations induces granular jamming
- Cohesive bonds can provide similar behavior as Coulomb frictional parameterizations
- A probabilistic model characterizes the likelihood of jamming over time

Correspondence to:
A. Damsgaard,
andersd@princeton.edu

Citation:
Damsgaard, A., Adcroft, A., & Sergienko, O. (2018). Application of discrete element methods to approximate sea ice dynamics. *Journal of Advances in Modeling Earth Systems*, *10*, 2228–2244. https://doi.org/10.1029/2018MS001299

Received 14 FEB 2018
Accepted 15 AUG 2018
Accepted article online 21 AUG 2018
Published online 11 SEP 2018

Abstract Lagrangian models of sea ice dynamics have several advantages over Eulerian continuum models. Spatial discretization on the ice floe scale is natural for Lagrangian models and offers exact solutions for mechanical nonlinearities with arbitrary sea ice concentrations. This allows for improved model performance in ice-marginal zones, where sea ice is fragmented. Furthermore, Lagrangian models can explicitly simulate jamming processes that occur when sea ice moves through narrow confinements. While difficult to parameterize in continuum formulations, jamming emerges spontaneously in dense granular systems simulated in a Lagrangian framework. Here we present a flexible discrete element framework for approximating Lagrangian sea ice mechanics at the ice floe scale, forced by ocean and atmosphere velocity fields. Our goal is to evaluate the potential of models simpler than the traditional discrete element methods for granular dynamics. We demonstrate that frictionless contact models based on compressive stiffness alone are unlikely to produce jamming and describe two different approaches based on Coulomb friction and cohesion which both result in increased bulk shear strength of the granular assemblage. The frictionless but cohesive contact model displays jamming behavior which is similar to the more complex model with Coulomb friction and ice floe rotation at larger scales and has significantly lower computational cost.

1. Introduction

Sea ice influences the atmosphere and ocean at high latitudes and thus the state of the climate throughout the globe (e.g., Chiang & Bitz, 2005; Curry et al., 1995; Deser et al., 2000). In climate models, large-scale behavior of sea ice is typically simulated using (elastic-)viscous-plastic (e.g., Hibler, 1979; Hunke & Dukowicz, 1997; Thorndike et al., 1975) or elastic-plastic continuum models (e.g., Feltham, 2008; Girard et al., 2011; Rampal et al., 2016; Weiss et al., 2007). Observations show that sea ice deformation in shear zones exhibits anisotropic properties (e.g., Girard et al., 2009; Weiss & Schulson, 2009; Wilchinsky & Feltham, 2006). However, in continuum models shear zones are greatly affected by grid resolution and mesh orientation (e.g., de Borst, 1991; Rudnicki & Rice, 1975). The model behavior can be improved by using nonviscous rheologies and adaptive meshes (e.g., Girard et al., 2011; Rampal et al., 2016). Moreover, continuum formulations are generally not well suited for simulating the ice-marginal zone, where spatial variability in sea ice concentration and ice floe thickness causes strong changes in mechanical properties. In such circumstances, continuum models do not simulate advection of a diverse ice pack correctly (e.g., Horvat & Tziperman, 2015).

1.1. Sea Ice as a Granular Material

Previous studies argued that sea ice can be treated as a granular material, with a bulk rheology determined by the local mechanics and geometry of discrete and interacting ice floes (e.g., Bak et al., 1988; Coon, 1974; Feltham, 2005; Hopkins, 2004; Hopkins & Thorndike, 2006; Tremblay & Mysak, 1997). In granular materials this behavior is called *self-organized complexity* as the overall behavior is governed by the local interactions and the resultant many-body response of the system (e.g., Bak et al., 1988). Examples of granular phenomena include jets of sea ice floes in the marginal ice zone (e.g., Feltham, 2005) and jamming (Herman, 2013; Kwok et al., 2010; Rallabandi et al., 2017a, 2017b; Samelson et al., 2006). Mechanical rigidity of granular materials increases with the grain-packing density. Granular systems *jam* when this strengthening exceeds the driving stress, for example, during flow through narrow conduits (e.g., Cates et al., 1998; To et al., 2001; Zuriguel, 2014). In the cryosphere jamming is observed and modeled in icebergs in Greenlandic fjords (Peters et al., 2015; Robel, 2017) and controls the sea ice flux through narrow confinements such as the Nares Strait between Greenland and Canada (e.g., Kwok et al., 2010; Rallabandi et al., 2017a, 2017b). Granular materials have a highly nonlinear shear strength as a function of packing fraction or porosity. The nonlinear granular rheology

can cause jamming in continuum models (e.g., Rallabandi et al., 2017a, 2017b) but does not capture the uncertainty associated with the jamming process. A probabilistic model can describe the likelihood of granular jamming (e.g., Tang et al., 2009; Thomas & Durian, 2015). In the model proposed by Tang et al. (2009) the chance of survival P_s (the likelihood of the system to not undergo jamming) decreases exponentially with time t:

$$P_s = \exp(-t/T), \tag{1}$$

where the characteristic time scale of jamming T is dependent on the material, the experimental geometry, and the forcing. The Mohr-Coulomb frictional coefficient μ_u that links shear stress τ_u with compressive normal stress N controls the mechanics of dense assemblages of granular materials:

$$\tau_u = C + \mu_u N, \tag{2}$$

where C is the material cohesion. This relationship is well established for granular materials (e.g., Terzaghi et al., 1996) and ice (Feltham, 2008; Fortt & Schulson, 2007, 2009; Schulson & Fortt, 2012; Schulson et al., 2006; Weiss et al., 2007). The effect of inertia on the postfailure rheology is described by the magnitude of the dimensionless inertia number I:

$$I = \dot{\gamma}\bar{d}\sqrt{\frac{\rho}{N}}, \tag{3}$$

where $\dot{\gamma}$ is the shear strain rate, $\bar{d}$ is the representative grain diameter, and ρ is the grain density. For low values of the inertia number ($I \lesssim 10^{-3}$), granular rheology is essentially rate independent, and the Mohr-Coulomb frictional coefficient μ_u and dilative response is constant (e.g., GDR-MiDi, 2004). For values of $I \gtrsim 10^{-3}$, granular materials behave as viscoplastic *Bingham materials*, with the frictional coefficient depending in a nonlinear fashion on the inertia number (da Cruz et al., 2005; Forterre & Pouliquen, 2008; GDR-MiDi, 2004; Jop et al., 2006), that is, $\tau_u = \mu_u(I)N$. However, the $\mu_u(I)$ rheology does not include effects of nonlocality (e.g., Henann & Kamrin, 2013), and, therefore, deformation is not distributed through material-dependent shear zones of finite width. Dilation represents an additional complexity to granular shear zones with rigid particles and is induced in dense packings as grains need space for relative movement (e.g., Nedderman, 1992; Reynolds, 1885; Terzaghi et al., 1996; Tremblay & Mysak, 1997; Wilchinsky et al., 2010, 2011). The magnitude of dilation depends on material properties and the applied forcing (e.g., Aharonov & Sparks, 2002; Damsgaard et al., 2013). Continuum modeling of dry and cohesionless granular materials is an area of active research and debate (e.g., Bouzid et al., 2013; da Cruz et al., 2005; Forterre & Pouliquen, 2008; Henann & Kamrin, 2013; Jop et al., 2006). For this reason we use particle-based Lagrangian methods for our sea ice modeling, as individual ice floe contact mechanics are more established than continuum rheologies.

1.2. Numerical Methods for Granular Materials

The discrete element method (DEM, also known as the *distinct element method*) is widely used to model granular media and discontinuous materials in a variety of contexts (e.g., Radjaï & Dubois, 2011). The most popular approach is the *soft body* DEM, originally derived from molecular dynamics modeling principles by Cundall and Strack (1979), where grain kinematics are determined by explicit temporal integration of their momentum balance. The DEM has been applied with discretizations on the sub-ice floe scale (Hopkins et al., 1991) or with particles representing a collection of ice floes (Li et al., 2014). Thus far, for sea ice modeling the DEM is typically applied to simulate one ice floe per particle (e.g., Gutfraind & Savage, 1997a; Herman, 2016; Hopkins, 2004).

However, the DEM and other Lagrangian approaches to modeling sea ice dynamics have not been used as components of global climate models because of high computational expense. Sea ice models based on smoothed-particle hydrodynamics have been proposed (e.g., Gutfraind & Savage, 1998; Lindsay & Stern, 2004), which offer better computational performance and Lagrangian discretizations. However, the complexity and kinematic phase transitions of granular materials are difficult to generalize in continuum formulations required for Eulerian models and smoothed-particle hydrodynamics approaches (e.g., Aharonov & Sparks, 1999; Bouzid et al., 2013; da Cruz et al., 2005; GDR-MiDi, 2004; Gutfraind & Savage, 1997b; Monaghan, 2012).

The DEM is generally a computationally intensive approach. Due to the Lagrangian nature of the method, sophisticated neighbor search algorithms are required to minimize the computational cost of contact mapping. Furthermore, the explicit temporal integration of the per-grain momentum balance is determined by

the elastic wave speed through the granular assemblage and thus requires short time steps for attaining numerical stability (e.g., Kruggel-Emden et al., 2008, Radjaï & Dubois, 2011),

$$\Delta t \leq \frac{\epsilon}{\sqrt{\frac{\max(k_n)}{\min(m)}}}, \tag{4}$$

where ϵ is a safety factor (e.g., $\epsilon = 0.07$), $\max(k_n)$ is the largest elastic stiffness in the system, and $\min(m)$ is the smallest particle mass. As apparent from equation (4), small ice floes require small time steps, while softening of the elastic modulus can speed up the computations. In order to increase the computational efficiency, it is common in DEM applications to both remove smaller grains and reduce the elastic stiffness of the grains, resulting in an increased time step length. The effect of these modifications can be assessed by evaluating the inertia number (equation (3)). If it remains in the rate-independent regime of $I \lesssim 10^{-3}$, a grain size increase and/or elastic softening will be inconsequential for the overall strength and dilative behavior of the granular system. If $I > 10^{-3}$ the shear stress and dilation will increase nonlinearly with increasing shear strain rate (e.g., da Cruz et al., 2005; GDR-MiDi, 2004). However, the DEM time step (subseconds to tens of seconds) is generally much shorter than climate model time steps (minutes to hours).

The goal of this study is to develop a numerical approach for simulating sea ice on the individual floe scale, which, at the same time, is computationally efficient enough to be used as a component of a climate model (e.g., Delworth et al., 2006; Gnanadesikan et al., 2006; Griffies et al., 2005). To do so, we make methodological simplifications relative to other discrete element studies on sea ice and explore the large-scale implications of different choices of contact rheology.

2. Methods

2.1. Governing Equations

For computational efficiency, we treat the ice floes as cylinders moving in two dimensions along the atmosphere-ocean interface. The ice floe geometry is described by thickness h and horizontal radius r. The translational momentum balance for an ice floe with index i is

$$m^i \frac{\mathrm{D}^2\mathbf{x}^i}{\mathrm{D}t^2} = \underbrace{\sum_j \left(\mathbf{f}_n^{ij} + \mathbf{f}_t^{ij}\right)}_{\text{Contact forces}} + \mathbf{f}_o^i + \mathbf{f}_a^i, \tag{5}$$

where m is the ice floe mass, $\mathbf{x}$ is ice floe center position, and $\mathbf{f}_n$ and $\mathbf{f}_t$ is granular contact-normal and tangential force from interaction with ice floe j. The external forces $\mathbf{f}_o$ and $\mathbf{f}_a$ are ocean- and atmosphere-induced drag, respectively. Similarly, the angular momentum balance for grain i is

$$J_z^i \frac{\mathrm{D}^2\Omega^i}{\mathrm{D}t^2} = \underbrace{\sum_j \left(r^i \mathbf{n}^{ij} \times \mathbf{f}_t^{ij}\right)}_{\text{Contact torques}} + t_o^i + t_a^i. \tag{6}$$

J_z is the moment of inertia around the vertical center axis, and Ω is the angular position of ice floe i. The contact-normal unit vector is denoted $\mathbf{n}_{ij}$. The ocean and atmosphere can induce rotational torques t_o and t_a due to floe vorticity or ice floe rotation. The forces and torques that appear in the linear and angular momentum balances are described below. In this study, and in the above equations for momentum, we disregard Coriolis forces, sea surface slope, or wave action. These terms should be considered when implementing in coupled models but are omitted here due to the idealized ocean and atmosphere in our simulation setups. We integrate the momentum balance equations in time using a third-order Taylor expansion scheme, which is computationally simple and has a high level of numerical precision (e.g., Kruggel-Emden et al., 2008).

In this study, we compare the jamming behavior of two differing ice floe contact models. Common to both models is $\mathbf{f}_n$, the resistive force to axial compressive strain between to cylindrical ice floes i and j, which is modeled by (Hookean) linear elasticity based on the overlap distance δ_n:

$$\mathbf{f}_n^{ij} = A^{ij} E^{ij} \delta_n^{ij} \quad \text{when} \quad 0 > |\delta_n^{ij}| \equiv |\mathbf{x}^i - \mathbf{x}^j| - (r^i + r^j). \tag{7}$$

This is a common approach in discrete element simulations (e.g., Cundall & Strack, 1979; Damsgaard et al., 2016, 2017; Ergenzinger et al., 2011; Luding,). The contact cross-sectional area $A^{ij} = R^{ij}\min(h^i, h^j)$ is determined by the harmonic mean $R^{ij} = 2r^i r^j/(r^i + r^j)$ of the ice floe radii r^i and r^j, as well as the smallest of the involved ice floe thicknesses h^i and h^j. The harmonic mean of Young's modulus E^{ij} scales the linear elastic force resulting from axial strain of a distance $|\delta_n^{ij}|$. The stiffness is scale invariant (e.g., Obermayr et al., 2013) and assumes constant elastic properties of the ice itself, regardless of ice floe size. We note that nonlinear elasticity models based on Hertzian contact mechanics may alternatively be applied to determine the stresses resulting from contact compression (e.g., Herman, 2013, 2016). However, with nonlinear stiffness models the numerical stability of the explicit temporal integration scheme depends on the stress and packing state of the granular assemblage and will under compressive stress extremes require very small time steps. In the simulations in this study, we use a Young's modulus of $E = 2.0 \times 10^7$ Pa. This value is lower than what is observed for ice (e.g., Petrovic, 2003; Schulson, 1999) but strikes a reasonable balance between elastic compressibility and computational efficiency.

As we demonstrate below, models based on compressive strength alone result in a weak sea ice pack and are not sufficient to cause granular jamming. We explore two modifications to the contact model presented in equation (7). The first approach is typical to DEM models and is based on resolving shear resistance through tangential (contact parallel) elasticity, not exceeding the Coulomb frictional limit. An alternative approach, fundamentally complementary to compressive elasticity and shear friction, is tensile strength of ice floe contacts which leads to a cohesive bulk granular rheology.

2.2. Tangential Elasticity With Coulomb Friction

DEM models typically include resistance against slip between particles, by limiting relative tangential movement for interparticle contacts (e.g., Cundall & Strack, 1979). Tangential elasticity is resolved by determining the contact transverse travel distance $\boldsymbol{\delta}_t$ (i.e., the vector of shear motion) on the contact plane for the duration of the contact t_c:

$$\boldsymbol{\delta}_t^{ij} = \int_0^{t_c} \left[(\mathbf{v}^i - \mathbf{v}^j) \cdot \hat{\mathbf{t}}^{ij} - R^{ij}\left(\omega^i + \omega^j\right)\right], \tag{8}$$

where $\mathbf{v}$ and ω denote linear and angular velocity, respectively. The contact-parallel unit vector is denoted $\hat{\mathbf{t}}$. The contact transverse travel distance $\boldsymbol{\delta}_t$ is corrected for contact rotation over the duration of the interaction and is used to determine the contact-tangential elastic force:

$$\mathbf{f}_t^{ij} = \frac{E^{ij}A^{ij}}{R^{ij}} \frac{2(1-(\nu^{ij})^2)}{(2-\nu^{ij})(1+\nu^{ij})} \boldsymbol{\delta}_t^{ij}, \tag{9}$$

where ν^{ij} is the harmonic mean of the Poisson's ratios set for the ice floes. We use a constant value of $\nu = 0.185$ (Hopkins, 2004). Coulomb friction on the grain surface limits the tangential force, relative to the magnitude of the normal force:

$$|\mathbf{f}_t^{ij}| \leq \mu^{ij}|\mathbf{f}_n^{ij}|. \tag{10}$$

The Coulomb frictional coefficient μ introduced above describes resistance to sliding along the individual *grain surfaces* and should not be mistaken for the *bulk* Mohr-Coulomb frictional coefficient μ_u (equation (2)) that describes frictional behavior of an assemblage of many grains. In the case of slip ($|\mathbf{f}_t| > \mu|\mathbf{f}_n|$) the length of the contact transverse travel distance $\boldsymbol{\delta}_t$ reduces to be consistent with the Coulomb limit. This loss in energy storage accounts for tangential contact plasticity and irreversible work associated with contact sliding. Since the above model of tangential shear resistance is based on deformation distance on the interfloe contact plane, it requires solving for ice floe rotational kinematics of each ice floe and a bookkeeping algorithm for storing contact histories.

2.3. Tensile Contact Strength

Cohesion (mechanical attraction between separating ice floes) is introduced by parameterizing resistance to extension beyond the overlap distance between a pair of ice floes (i.e., $\delta_n^{ij} > 0$). For actual ice floes, tensile strength can arise due to refreezing (e.g., Menge & Jones, 1993; Schulson, 2001). The general description of bond mechanics includes resistance to bond compression, tension, shear, twist, and rolling (e.g., Herman, 2016; Obermayr et al., 2013; Potyondy & Cundall, 2004). Here we explore the applicability of using bond resistance to *compression* and *tension* alone as mechanical components contributing to bulk granular shear strength. The calculations for doing so are simpler than for the elastic-plastic Coulomb friction described above.

We parameterize tensile strength by applying equation (7) for the extensive regime ($\delta_n > 0$). Equation (7) is enforced until the tensile stress exceeds the tensile strength σ_c defined for the bonds:

$$|\mathbf{f}_n^{ij}| \leq \min(\sigma_c^i, \sigma_c^j) A^{ij}. \tag{11}$$

Cross-sectional area of the contact is found as $A^{ij} = R^{ij} \min(h^i, h^j)$ as in equation (7). The bond failure corresponds to Herman (2016) where a complete loss of tensile stress occurs when the tensile strength is exceeded. This is different from the linear decrease in stress after failure parameterized in Hopkins (2004) and Hopkins and Thorndike (2006).

Hopkins (2004) establishes full tensile strength for the ice pack once every 24-hr cycle. Here we set the bonds to obtain full tensile strength as soon as a pair of ice floes first undergoes compression ($\delta_n < 0$). Time-dependent strengthening ($\sigma_c(t)$ and $d\sigma_c/dt > 0$) causes a strain rate weakening that is not of immediate interest for this study.

2.4. Drag From Ocean and Atmosphere

We adapt v^2-type parameterizations for characterizing Stokes drag forces between ice floes and ocean or atmosphere. This approach is common in both Lagrangian and Eulerian models (e.g., Herman, 2016; Hopkins, 2004; Rallabandi et al., 2017a),

$$\mathbf{f}_o^i = \pi \rho_o \left(c_{v,o} 2 r^i D^i + c_{h,o} (r^i)^2 \right) (\mathbf{v}_o - \mathbf{v}^i) |\mathbf{v}_o - \mathbf{v}^i|, \tag{12}$$

where we use an idealized value of $\rho_o = 1 \times 10^3$ kg/m^3 as ocean density, D is the ice floe draft (here set to $D^i = 9h^i/10$), and $c_{v,o} = 0.14$ and $c_{h,o} = 1.6 \times 10^{-4}$ are vertical and horizontal drag coefficients (e.g., Gladstone et al., 2001; Martin & Adcroft, 2010), compatible with typical values in sea ice modeling (e.g., Hopkins, 2004). The ocean velocity is $\mathbf{v}_o$, and ice floe velocity is $\mathbf{v}$. Similarly, for the atmosphere-induced drag,

$$\mathbf{f}_a^i = \pi \rho_a \left(c_{v,a} 2 r^i (h^i - D^i) + c_{h,a} (r^i)^2 \right) (\mathbf{v}_a - \mathbf{v}^i) |\mathbf{v}_a - \mathbf{v}^i|. \tag{13}$$

The atmosphere density is $\rho_a = 1.3$ kg/m^3. The vertical and horizontal drag coefficients are $c_{v,a} = 0.064$ and $c_{h,a} = 8.0 \times 10^{-5}$, respectively. The wind velocity is $\mathbf{v}_a$. The curl of the ocean or atmosphere velocities ($\nabla \times \mathbf{v}_f$) induces a rotational torque (t) on the ice floes (e.g., Nakayama & Boucher, 1998), sometimes ignored in DEM sea ice models:

$$t_o^i = \pi (r^i)^4 \rho_o \left(\frac{r^i}{5} c_{h,o} + D^i c_{v,o} \right) ((\nabla \times \mathbf{v}_o)/2 - \omega^i) |(\nabla \times \mathbf{v}_o)/2 - \omega^i|, \tag{14}$$

and

$$t_a^i = \pi (r^i)^4 \rho_o \left(\frac{r^i}{5} c_{h,a} + (h^i - D^i) c_{v,a} \right) ((\nabla \times \mathbf{v}_a)/2 - \omega^i) |(\nabla \times \mathbf{v}_a)/2 - \omega^i|, \tag{15}$$

where ω is the ice floe angular velocity. The above terms add rotational drag for a spinning ice floe and can induce rotation for ice floes in ocean or atmosphere fields with high vorticity. Ocean and atmosphere curl may be reasonable to neglect on the ice floe scale (e.g., Herman, 2016) but are included here nonetheless.

2.5. Boundary Conditions

The domain boundaries can interact with the granular assemblage in a variety of ways. Ice floes are disabled from mechanical interaction with the rest of the ice floes when crossing an *inactive boundary*. Ice floes can interact mechanically across opposite sides of the model domain if the edges are *periodic boundaries* and are immediately repositioned to the opposite side if they cross a domain edge. *Fixed boundaries* are created by placing ice floes along a line and keeping them fixed in space. Optionally, the fixed grains can move at prescribed velocities. The free-moving ice floes undergo the same mechanical interactions with the fixed ice floes as used for their internal interactions. For the cohesive model, tensile bonds between free and fixed ice floes effectively create landfast ice areas. Finally, flat and frictionless walls can provide *normal stress boundaries* to the granular assemblage. These walls attempt to fulfill a certain contact stress normal to their geometric orientation and move through time to uphold the prescribed stress. They are assigned a constant mass, and their kinematics are resolved with explicit temporal integration of their stress balance, similar to the temporal integration performed for the ice floes themselves.

2.6. Model Limitations

The presented model is not sufficiently general for being a complete formulation for sea ice mechanics. For example, we do not include a parameterization of pressure ridging, important for mechanical redistribution of ice mass in converging regimes (e.g., Flato & Hibler, 1995; Hibler, 1980; Hopkins et al., 1991; Lipscomb et al., 2007; Rothrock, 1975; Thorndike et al., 1975). Furthermore, the ice floe shape is highly simplified as we neglect geometrical anisotropy and associated mechanical effects (e.g., Feltham, 2008; Hopkins, 2004; Wilchinsky & Feltham, 2006; Wilchinsky et al., 2011). However, direct modeling of polygonal sea ice floes is computationally excessive in the targeted context. Here we focus on differences between simple DEM models with the fewest additional layers of abstraction. Consequentially, the simulation results should not be compared directly to real settings, as further analysis and model development is required to do so.

The components of interaction on the ice floe scale influence the bulk behavior under various settings and forcings. The interaction described in the previous is typical for DEM implementations for sea ice in the literature (e.g., Herman, 2016; Hopkins, 1996, 2004).

3. Numerical Model

3.1. Implementation

We implement the model described above as a stand-alone and purpose-built DEM sea ice model `Granular.jl` (Damsgaard, 2018a). In this study we use drag from prescribed ocean and atmosphere velocity fields and explore strengths and limitations of different methods related to sea ice mechanics. A separate online repository contains the simulation scripts (Damsgaard, 2018b).

The effects of the ocean and atmosphere are here prescribed as constant velocity fields. The interpolation to the discrete ice floes is determined with bilinear interpolation to the ocean and atmosphere grids. The relative importance of neighboring grid points decreases linearly with distance. Ice floe contacts are detected by binning the population of ice floes with in a grid, where the cell width equals the largest ice floe diameter. All contacts for an ice floe can reliably be detected by searching for overlaps within the current and eight neighboring cells. Ice floes are transferred between the cell lists according to their movement through the sorting grid. This approach significantly reduces the computational overhead ($\mathcal{O}(n)$) compared to all-to-all contact searches ($\mathcal{O}(n^2)$) (e.g., Ericson, 2005). We do not include thermodynamic processes, and ice floe geometries do not change over the course of each simulation.

3.2. Experiments

We perform two types of experiments in order to understand the granular rheology and its applicability to simulate sea ice dynamics. In both cases we generate ice floe sizes by a power law distribution within the range r_{min} to r_{max} with an exponent of value −1.8, commonly used for describing sea ice in the marginal zone (e.g., Herman, 2010, 2013; Steer et al., 2008). For the experiments we parameterize the granular interaction in one of two ways:

1. *Coulomb frictional DEM*: linear elastic resistance to compressive strain normal to the contact interface (equation (7)) and linear elastic resistance to shear strain on the contact interface, with Coulomb friction limiting the tangential force magnitude (equation (10)). The kinematics are resolved with the translational and rotational momentum equations (equations (5) and (6)).
2. *Cohesive DEM*: linear elastic resistance to compressive strain normal to the contact interface (equation (7)) and linear elastic resistance to extensional strain between a bonded ice floe pair with a breakage criterion (equation (11)). The kinematics are resolved for translation only (equation (5)). Rotation (equation (6)) and contributing components (equations (8)–(10), (14), and (15)) are ignored.

Approach 1 requires that rotational kinematics of the ice floes are resolved (equation (6)) for correctly determining the tangential contact displacement (equation (8)). Including rotation approximately doubles the kinematic degrees of freedom and required computations. Approach (2) is computationally cheaper as it does not require resolving rotation (the ice floes are effectively frictionless). Without friction, the bulk shear strength is provided by geometrical roughness in the granular contact network. Cohesion further strengthens the granular topology and adds increased bulk resistance to deformation. The Coulomb frictional model (approach 1) is the standard method for simulating cohesionless granular materials and will for our purposes serve as a benchmark for testing the applicability of the less complex cohesive model (approach 2). We expect that the bulk mechanics for the two models can be similar in certain settings but differ in others as the micromechanical behavior is fundamentally different.

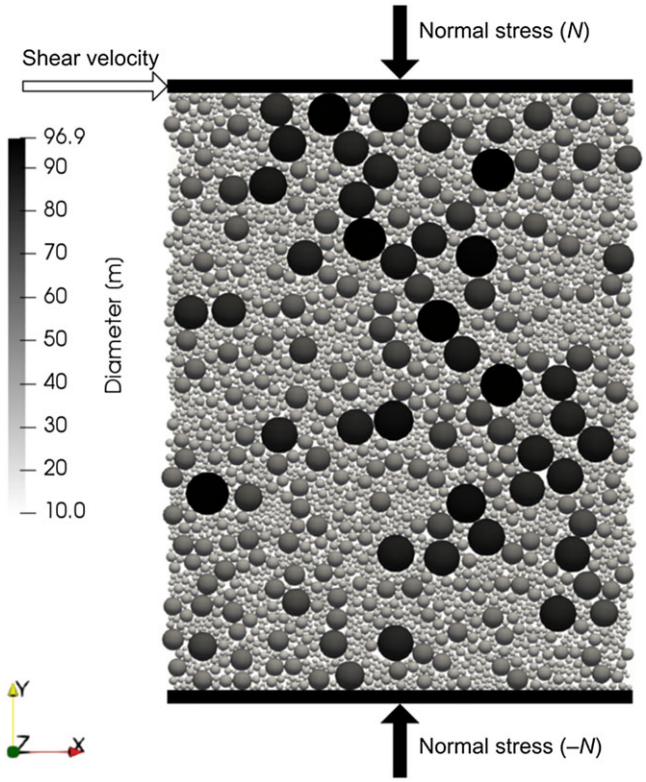

Figure 1. Simulation setup for the simple shear experiments. The upper and lower walls exert a prescribed normal stress to the granular assemblage, and a constant velocity along x is enforced for the uppermost ice floes. Left and right ($-x$ and $+x$) boundaries are periodic.

3.2.1. Simple Shear

We perform simple shear experiments on dense granular packings, where the ice floes are sheared from a preconsolidated state under a constant normal stress (Figure 1). The primary objective of these experiments is to validate the Mohr-Coulomb frictional behavior typical for granular materials (equation (2); e.g., Nedderman, 1992) and assess how the type of grain-to-grain contact rheology influences bulk stress properties. In the shear experiments we do not include ocean and atmosphere drag, as we are interested in analyzing the ice floe mechanics alone.

We adapt a simple-shear setup with boundary conditions typical in DEM modeling (e.g., Damsgaard et al., 2013), with a schematic overview in Figure 1. We initially generate ice floes with radii between 5 and 50 m in an irregular spatial arrangement without geometrical overlaps. We then apply a uniform ocean drag toward the lower boundary ($-y$) in order to increase the packing ratio. We then disable the ocean drag and perform

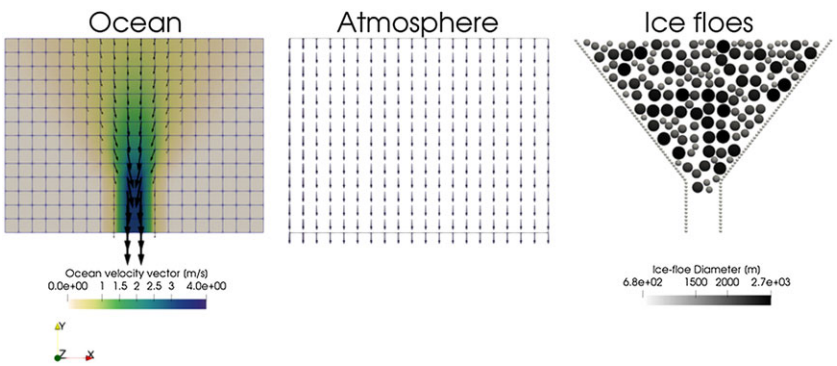

Figure 2. Simulation setup for the idealized strait experiments. Ocean velocities vary from 0 to 4 m/s relative to the bounding geometry, while the atmosphere velocity field is a uniform value of 30 m/s.

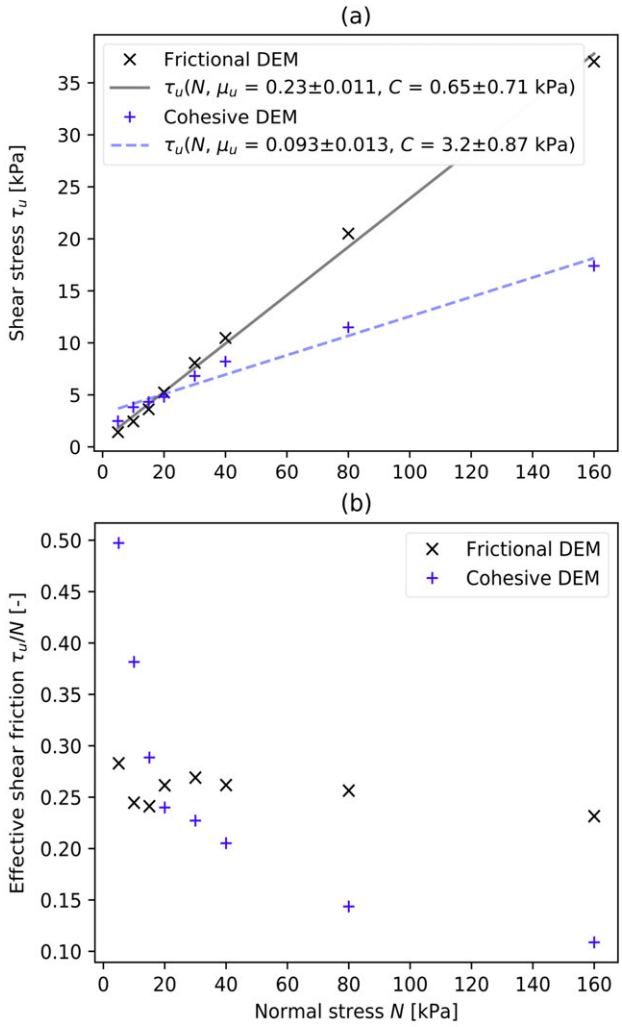

Figure 3. Steady state stress and friction during simple shear for Coulomb frictional model runs ($\mu = 0.3$ and $\sigma_c = 0$ kPa; see equations (10) and (11)) and cohesive model runs ($\mu = 0$ and $\sigma_c = 200$ kPa). (a) The bulk shear stress τ_u increases linearly with the applied normal stress. We optimize equation (2) using a least squares fit and note parameter estimates and 95% confidence intervals in the legend. (b) Effective friction observed in the two model types. DEM = discrete element method.

a *consolidation step* in order to further uniaxially compress the packing in equilibrium with the stress forcing, as common in Mohr-Coulomb tests on granular materials (e.g., Bowles, 1992; Mitchell & Soga, 2005). The consolidation is performed by adding a normal stress boundary condition to the top (+y). Finally, we perform a constant-rate *shear step* by prescribing a velocity toward +x of 1 m/s to the grains just below the upper boundary (Figure 1). The bulk shear stress is determined from the sum of contact forces along y against the top grains. The side boundaries (−x and +x) are periodic in order allow arbitrary shear strains without geometrical constraints. Grains that are positioned within one grain size to the lower boundary (−y) are fixed in space in order to provide geometrical and mechanical roughness. The parameter choices result in granular inertia parameters in the range of $I = [10^{-3}; 10^{-2}]$ (equation (3)), so slight shear rate dependence on the observed bulk shear stress can be expected.

3.2.2. Jamming in Idealized Straits

In this set of experiments we use ocean and atmosphere drag to push the ice floes through a confining strait of funnel-shaped geometry (Figure 2) and analyze how the ice floe properties influences the likelihood of granular jamming. The geometry is similar to the ones from earlier studies focused on ice discharge with smoothed-particle dynamics and a discrete element model outside of the regime of granular jamming (Gutfraind & Savage, 1998). The ice floes are forced with wind and ocean current fields oriented from north to

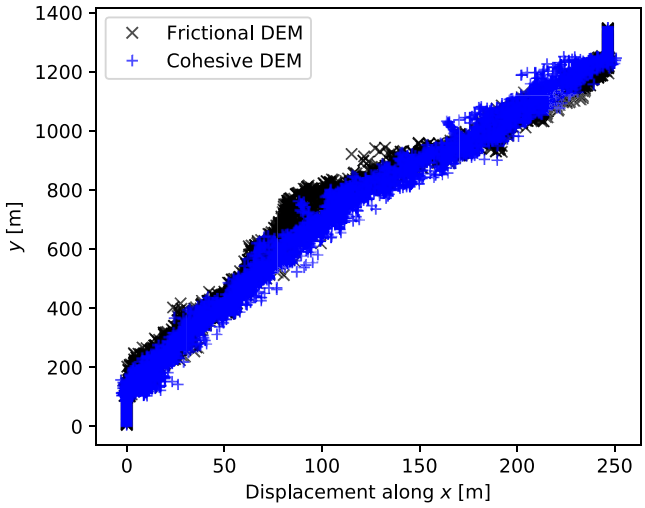

Figure 4. Ice floe displacements in the simple shear experiments with a normal stress of $N = 20$ kPa. DEM = discrete element method.

south. The spatial velocity pattern of the ocean is defined by a stream function, where the ocean flows through the confining strait with a velocity field consistent with mass conservation. Ice floes are initially placed in a pseudorandom arrangement north of the channel. During our initial tests we observed that the simulated material never jammed *inside* the flat-walled channel but always at or before the channel entrance. For that reason, we constrain our simulation domain size to only include the relevant parts.

New ice floes are continuously added to the top of the domain as soon as there is space to accommodate them. The sizes are drawn from the same power law size distribution. The bottom edge of the domain is an inactive boundary. During each experiment we determine the mass of disabled ice floes at the bottom as a measure of cumulative ice transport through the strait. If granular jamming occurs, ice floes stop reaching the bottom. We impose the criteria that the ice mass at the bottom must have been constant for more than 1 hr in simulation time for being classified as jammed. The experiments rely on pseudorandom number generation for generating ice floe size distributions, in order to obtain statistical description of the behavior (equation (1)). The radii are drawn between 600 and 1,350 m. We seed the pseudorandom number generation with different values and repeat each experiment 10 times with identical mechanical parameters to assess the statistical probability of granular jamming.

4. Results

In this section we compare bulk behavior between the algorithmically complex Coulomb frictional model and the simpler cohesive model. The supporting information contains animations of the shear and jamming experiments.

A benchmark of the computational performance reveals that the interaction routine is 2.1 times faster for the cohesive model relative to the Coulomb frictional model. By avoiding rotation, kinematic degrees of freedom are in our two-dimensional (2-D) setup reduced from 9 to 6 for the cohesive model. The models have identical requirements for the granular contact search, so performance here is not improved.

4.1. Simple Shear

We observe that both the Coulomb frictional and cohesive models follow the Mohr-Coulomb constitutive relation (equation (2)), as the bulk shear stress of the granular assemblages τ_u scales linearly with normal stress N applied normal to the shear direction (Figure 3a). The Coulomb frictional model produces an ice floe pack with a small value for bulk cohesion (C) and a strong linear correlation between normal stress and shear stress. The cohesive model results in an ice floe pack with a higher bulk cohesion, but it also shows increasing shear stresses with increasing normal stress. There is a reasonable overlap in shear stress between the two models at $N \in [5; 40]$. However, the bulk friction is not the same across a larger range of N because of the different micromechanical assumptions of the two models.

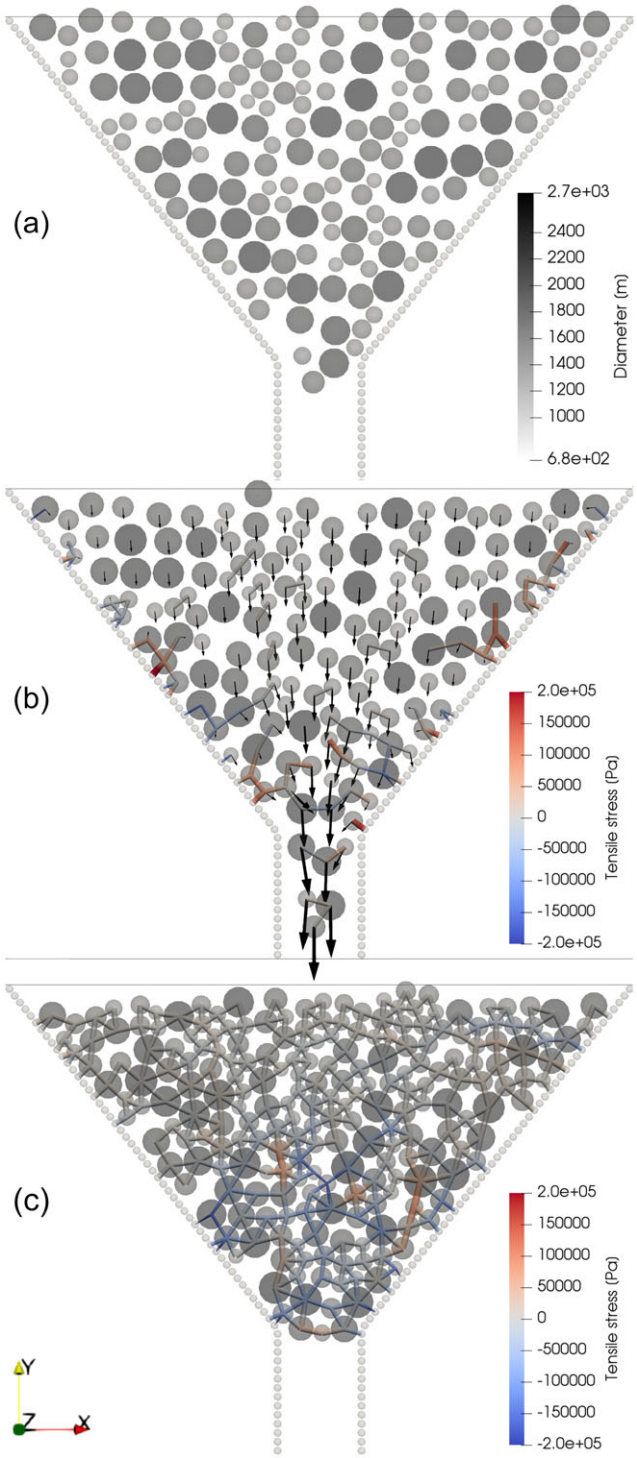

Figure 5. Example visualization of the granular system for the *idealized strait* runs, here the initial state (a), during flow (b), and in a jammed state (c). Black arrows denote the linear velocity of the ice floes, and colored bars indicate compressive or tensile granular interactions. The above visualizations are for run 1 out of 10 with $\mu = 0$ and $\sigma_c = 400$ kPa.

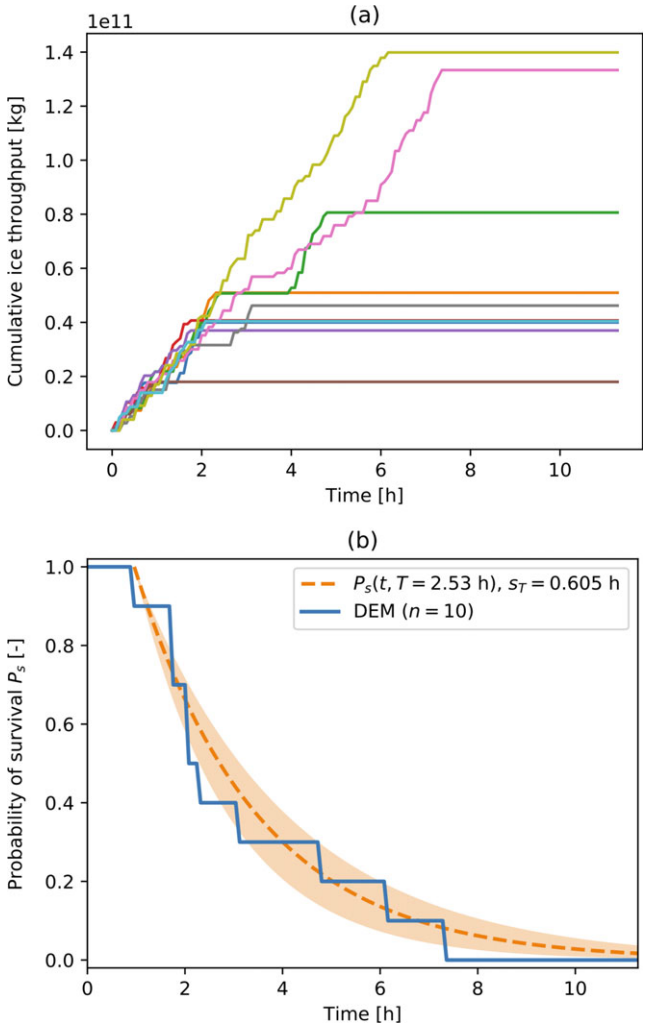

Figure 6. (a) The cumulative mass of ice flushed through the idealized strait over time in experiments of identical mechanical parameters (cohesive model, $\mu = 0$ and $\sigma_c = 400$ kPa) but with random perturbations to the initial ice floe placements and sizes. (b) Probability of survival (nonjamming) P_s for the ensemble in (a), with a corresponding least squares fit of equation (1). The legend shows the best fit value for the characteristic jamming time T, as well as the sample standard deviation around the mean. DEM = discrete element method.

The effective shear friction (τ_u/N) is a metric that describes bulk mechanical properties during shear (Figure 3b). For the Coulomb frictional tests, we see that the bulk frictional coefficient ($\mu_u \approx 0.25$, equation (2) is lower than the Coulomb frictional coefficient we parameterize on the contact level ($\mu = 0.3$, equation (10). Ice floe rotation decreases the bulk strength, which is common for 2-D granular systems with circular grains. The Coulomb frictional model retains most of its effective friction under the tested range of normal stresses (Figure 3b), in line with observations of sea ice mechanics (e.g., Fortt & Schulson, 2007; Schulson et al., 2006; Weiss et al., 2007). In contrast, the cohesive model becomes monotonically weaker under larger normal stresses, with a large decrease in the lower range of N. While strong cohesion is expected to localize failure, the distribution of shear strain (Figure 4) is similar in the two models. The only difference is that shear strain is slightly more localized toward the moving boundary in the Coulomb frictional DEM and more linear and distributed in the cohesive DEM.

4.2. Jamming in Idealized Straits

By adjusting the grain-to-grain frictional coefficient μ (equation (10)) and the tensile strength σ_c (equation (11)), we can assess jamming tendencies in the two models Figure 5 shows our setup where atmosphere and ocean force ice floes through an idealized strait. Figure 6a shows that the time to jamming is strongly influenced by small variations in initial ice floe configurations. With the applied contact parameters ($\mu = 0$ and $\sigma_c = 400$ kPa), all 10 runs jam after a period of ~7 hr. We plot the ratio of survived (nonjammed) runs

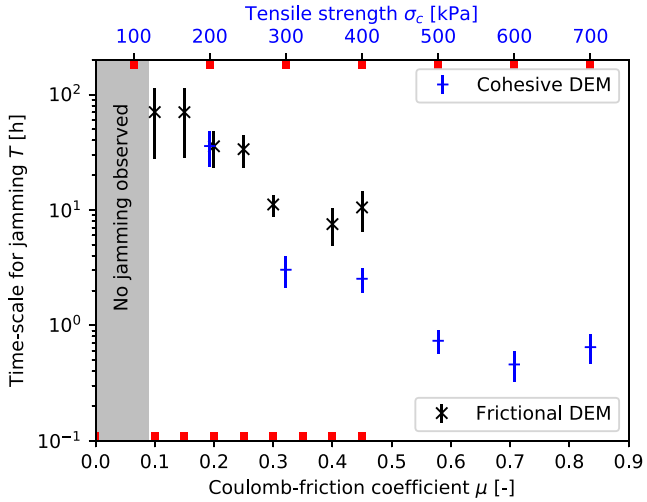

Figure 7. The influence of the Coulomb frictional coefficient μ (equation (10)) and the tensile strength σ_c (equation (11)) on the characteristic time for jamming T (equation (1)) through a strait of width $W = 6{,}000$ m. A statistically significant fit could not be achieved from the Coulomb frictional ensemble with $\mu = 0.35$. Red ticks denote tested values. DEM = discrete element method.

as a function of time (Figure 6b) and fit an exponential decay function to the survival fraction (Tang et al., 2009, equation 1) with the Levenberg-Marquardt algorithm of nonlinear least squares optimization. The decay time scale parameter T and the sample standard deviation s_T are useful metrics for comparing the effect of different prescribed properties to the jamming behavior of the ice pack system. We offset the curve fit in time corresponding to the first occurrence of jamming.

We observe that larger friction coefficients μ increase the mechanical rigidity and increase the likelihood of jamming in the Coulomb frictional model with rotation (Figure 7, black ticks). Similarly, increases in grain-to-grain tensile strength increases the likelihood of jamming in the reduced-complexity model with cohesion (Figure 7, blue ticks). Neither model displays jamming as the system becomes frictionless ($\mu \to 0$) or cohesionless ($\sigma_c \to 0$), highlighting the need for including interactions other than contact-normal elastic repulsion (equation (7)). Due to the monotonic nature of the jamming time scale in both models, we can determine a value for the tensile strength σ_c that with the cohesive model corresponds to the jamming behavior of a certain μ value for the Coulomb frictional model (or vice versa). The jamming behavior is broadly similar

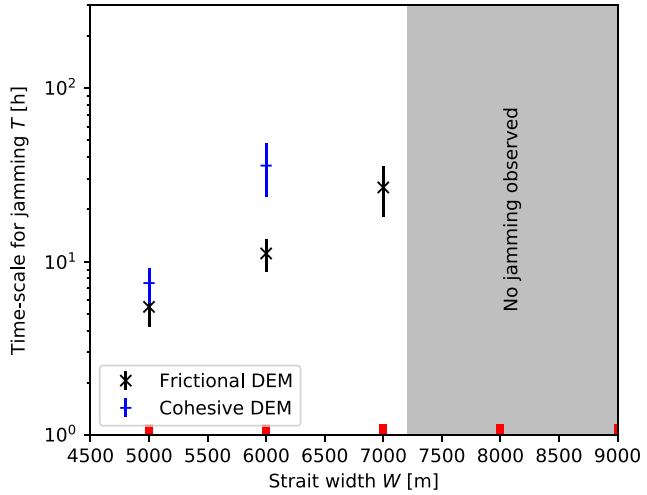

Figure 8. Jamming behavior with increasing width of the strait (Figure 5) for Coulomb frictional ($\mu = 0.3$ and $\sigma_c = 0$ kPa) and cohesive runs ($\mu = 0$ and $\sigma_c = 200$ kPa). The frictional model does not show jamming above $W = 7{,}000$ m, and the cohesive model does not show jamming above $W = 6{,}000$ m. Red ticks denote tested values. DEM = discrete element method.

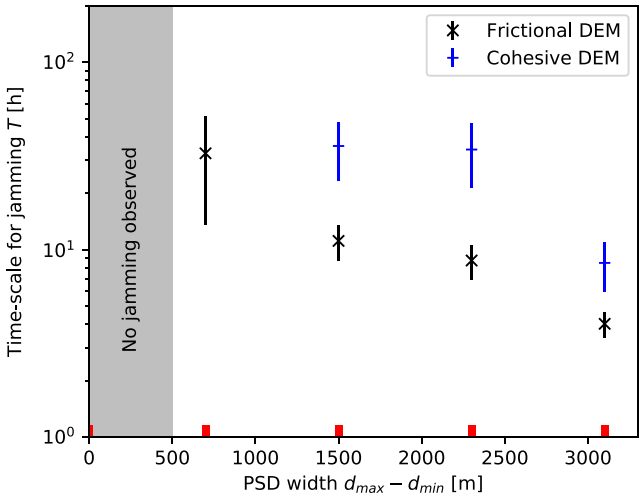

Figure 9. Jamming behavior with increasing width of the particle size distribution for Coulomb frictional ($\mu = 0.3$ and $\sigma_c = 0$ kPa) and cohesive runs ($\mu = 0$ and $\sigma_c = 200$ kPa). Red ticks denote tested values. DEM = discrete element method.

for the Coulomb frictional model with $\mu = 0.3$ and $\sigma_c = 0$ kPa, and the cohesive model with $\mu = 0$ and $\sigma_c = 200$ kPa (Figures 7a and 7b).

In both models, jamming does not occur across straits that are wide with respect to grain size, consistent with the expectation of constant granular discharge across wide confinements (Figure 8). As strait width decreases, the jamming time scale T decreases in a nonlinear fashion for both the Coulomb frictional and cohesive models. With the applied parameters the Coulomb frictional model was able to jam in straits of width $W = 7{,}000$ m, while the cohesive model only displayed jamming up to $W = 6{,}000$ m.

We also increase the width of the generated particle size distribution around the same mean value and observe that jamming occurs faster in wide size spans (Figure 9). While smaller ice floes act as lubricants facilitating flow, larger ice floes provide structural rigidity leading to eventual jamming. It is primarily the advection of larger ice floes to the strait entrance that causes the jamming itself. In the Coulomb frictional model, ice floe thickness does not directly influence jamming behavior (Figure 10), as the presented implementation adjusts stress-based yield criteria for contact sliding and tensile bond breakage accordingly. However, the cohesive model displays increased likelihood of jamming with increased thicknesses, similar to previous studies of ice bridge stability in confinements (Rallabandi et al., 2017b).

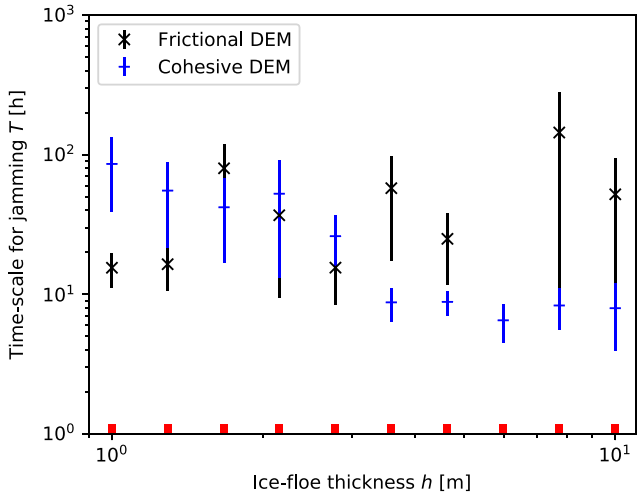

Figure 10. Jamming behavior with uniformly increasing thickness of the ice floes for Coulomb frictional ($\mu = 0.3$ and $\sigma_c = 0$ kPa) and cohesive runs ($\mu = 0$ and $\sigma_c = 200$ kPa). Red ticks denote tested values. DEM = discrete element method.

5. Discussion and Summary

We have developed a flexible discrete element framework for simulating Lagrangian sea ice dynamics at the ice floe scale, forced by ocean and atmosphere velocity fields. Frictionless contact models based on compressive stiffness alone are very unlikely to jam. We describe two different approaches based on Coulomb friction and tensile strength, where both additions result in increased bulk shear strength of the granular assemblage. We demonstrate that the discrete element approach is able to undergo granular jamming when forced through an idealized confinement, where the probability of jamming is determined by the channel width, ice floe thicknesses, and ice floe size variability. The frictionless but cohesive contact model can, with certain tensile strength values, display jamming behavior which on the large scale is broadly similar to a model with contact friction and ice floe rotation. However, the behavior of the two models is not exactly similar in other settings. During shear, the models show separate trends in bulk effective friction, and differing behavior is expected under pure divergent forcings.

Our results are consistent with previous studies on granular mechanics, specifically regarding how the magnitude of the Coulomb frictional coefficient influences bulk behavior. Morgan (1999) demonstrated that the particle-frictional coefficient increases bulk frictional strength of dense and 2-D systems up to a certain point where grain rolling becomes dominant over grain-to-grain contact sliding. Kamrin and Koval (2014) showed that particle surface friction affects bulk behavior and that increasing Coulomb frictional coefficients increase shear strength. Furthermore, and under certain conditions, the spatial distribution of shear deformation can be affected by the micromechanical grain friction. Morgan (2015) investigated the combined effects of Coulomb friction and tensile cohesion on the structural and mechanical evolution of fold and thrust belts and contractional wedges. In this study, broken bonds did not reform over time. It was observed that large tensile bond strengths caused increases in bulk shear strength, primarily by increasing the bulk cohesion in the Mohr-Coulomb constitutive relationship. Cohesion caused the material to behave in a rigid manner, with thin shear zones of broken bonds where bonds have failed. Without cohesion, deformation was more distributed in space. In our experiments, we observe similar behavior where increasing tensile strengths makes a dense ice pack behave like a rigid system (Figure 5c). However, our parameterization reforms bonds progressively when ice floes again come into contact, which limits the strain weakening otherwise associated with bond breaking.

The Coulomb frictional DEM model naturally strengthens in a linear manner with increasing compressive stress on the contacts (equation (10)), which linearly increases bulk shear strength (Figure 3a), as typical for granular materials tested in laboratory shear devices or when simulated with the DEM (e.g., Damsgaard et al., 2013; Morgan, 2015). The contacts of the cohesive model do not strengthen due to increased contact loading, which explains the weaker behavior observed at large normal stresses (Figure 3c). However, shear strength does still increase, since larger normal stresses on the shear zone cause self-arrangement into a denser packing. The dense system contains relatively more contacts with tensile strength, which on a bulk scale strengthens the mechanical resistance to shear. While cohesion can affect deformation patterns (e.g., Morgan, 2015) the shear profiles are not significantly different between the two profiles (Figure 4). We do not expect notable difference in deformation patterns on larger scales unless strong cohesion is applied.

The approach used in this study relies on many simplifications and is not capable of producing the richness of sea ice behavior observed in nature, in terms of both geometry and interaction. These limitations can be removed if computational efficiency is less than a central concern. Cylindrical or circular grain shape representations slightly reduce bulk shear strength relative to particles of irregular shape (e.g., Mair et al., 2002). In an attempt to compensate for shape-induced weakening, the Coulomb frictional coefficient or tensile strength can be increased in order to tend to the desired bulk mechanics. Furthermore, it may be beneficial to add random variation to mechanical properties (e.g., μ and σ_c) if the range of variability is well understood. Ice floe ridging is by crude means approximated by the bonding process described here, but it may be possible to improve the floe-scale mechanics for this process (e.g., Flato & Hibler, 1995; Lipscomb et al., 2007; Rothrock, 1975), especially if thermodynamic balance and the important process of refreezing is determined in conjunction with ocean and atmosphere state. Instead of attempting the impossible goal of including the entire details of the complex sea ice system, we intend for this parameterization to be a useful first attempt at making Lagrangian and ice floe scale methods available for coupled and global climate models. Lagrangian formulations have inherent advantages to continuum sea ice models, especially for handling the discontinuous behavior in shear zones and granular phenomena in the ice-marginal zone. We demonstrate that simplifications in DEM formulations can reduce the algorithmic complexity while retaining similar shear zone morphology and jamming behavior.

Acknowledgments
This work was supported by ExxonMobil through its membership in the Princeton E-filliates Partnership of the Andlinger Center for Energy and the Environment. Anders Damsgaard benefited from discussions with Alon A. Stern, Mitchell Bushuk, Michael Winton, and Behrooz Ferdowsi in preparation for this paper. We thank the reviewers and Associate Editor for constructive criticism which has greatly improved the content of this paper.

References

Aharonov, E., & Sparks, D. (1999). Rigidity phase transition in granular packings. *Physical Review E*, *60*(6), 6890–6896.
Aharonov, E., & Sparks, D. (2002). Shear profiles and localization in simulations of granular shear. *Physical Review E*, *65*, 051302.
Bak, P., Tang, C., & Wiesenfeld, K. (1988). Self-organized criticality. *Physical Review A*, *38*(1), 364–374. https://doi.org/10.1103/physreva.38.364
Bouzid, M., Trulsson, M., Claudin, P., Clément, E., & Andreotti, B. (2013). Nonlocal rheology of granular flows across yield conditions. *Physical Review Letters*, *111*(23), 187204. https://doi.org/10.1103/physrevlett.111.238301
Bowles, J. E. (1992). *Engineering Properties of Soils and their Measurement* (pp. 241). New York: Irwin/McGraw-Hill.
Cates, M. E., Wittmer, J. P., Bouchaud, J.-P., & Claudin, P. (1998). Jamming, force chains, and fragile matter. *Physical Review Letters*, *81*(9), 1841–1844. https://doi.org/10.1103/physrevlett.81.1841
Chiang, J. C. H., & Bitz, C. M. (2005). Influence of high latitude ice cover on the marine Intertropical Convergence Zone. *Climate Dynamics*, *25*(5), 477–496. https://doi.org/10.1007/s00382-005-0040-5
Coon, M. (1974). Mechanical behavior of compacted Arctic ice floes. *Journal of Petroleum Technology*, *26*(4), 466–470. https://doi.org/10.2118/3956-pa
Cundall, P. A., & Strack, O. D. L. (1979). A discrete numerical model for granular assemblies. *Géotechnique*, *29*, 47–65. https://doi.org/10.1680/geot.1979.29.1.47
Curry, J. A., Schramm, J. L., & Ebert, E. E. (1995). Sea ice-albedo climate feedback mechanism. *Journal of Climate*, *8*(2), 240–247. https://doi.org/10.1175/1520-0442(1995)008<0240:siacfm>2.0.co;2
da Cruz, F., Emam, S., Prochnow, M., Roux, J.-N., & Chevoir, F. (2005). Rheophysics of dense granular materials: Discrete simulation of plane shear flows. *Physical Review E*, *72*(2), 021309. https://doi.org/10.1103/physreve.72.021309
Damsgaard, A. (2018a). Granular.jl: Julia package for granular dynamics simulation (Version 0.3.2). https://doi.org/10.5281/zenodo.1165990
Damsgaard, A. (2018b). SeaIce-experiments: Simulation scripts using Granular.jl (Version 1.0.0). https://doi.org/10.5281/zenodo.1166005
Damsgaard, A., Cabrales-Vargas, A., Suckale, J., & Goren, L. (2017). The coupled dynamics of meltwater percolation and granular deformation in the sediment layer underlying parts of the big ice sheets. In *Proceedings of the 6th Biot conference on Poromechanics*. Paris, France: American Society of Civil Engineers. https://doi.org/10.1061/9780784480779.024
Damsgaard, A., Egholm, D. L., Beem, L. H., Tulaczyk, S., Larsen, N. K., Piotrowski, J. A., & Siegfried, M. R. (2016). Ice flow dynamics forced by water pressure variations in subglacial granular beds. *Geophysical Research Letters*, *43*, 12,165–12,173. https://doi.org/10.1002/2016gl071579
Damsgaard, A., Egholm, D. L., Piotrowski, J. A., Tulaczyk, S., Larsen, N. K., & Tylmann, K. (2013). Discrete element modeling of subglacial sediment deformation. *Journal of Geophysical Research: Earth Surface*, *118*, 2230–2242. https://doi.org/10.1002/2013JF002830
de Borst, R. (1991). Numerical modelling of bifurcation and localisation in cohesive-frictional materials. *Pure and Applied Geophysics*, *137*(4), 367–390.
Delworth, T. L., Broccoli, A. J., Rosati, A., Stouffer, R. J., Balaji, V., Beesley, J. A., et al. (2006). GFDL's CM2 global coupled climate models. Part I: Formulation and simulation characteristics. *Journal of Climate*, *19*(5), 643–674.
Deser, C., Walsh, J. E., & Timlin, M. S. (2000). Arctic sea ice variability in the context of recent atmospheric circulation trends. *Journal of Climate*, *13*(3), 617–633. https://doi.org/10.1175/1520-0442(2000)013<0617:asivit>2.0.co;2
Ergenzinger, C., Seifried, R., & Eberhard, P. (2011). A discrete element model to describe failure of strong rock in uniaxial compression. *Granular Matter*, *13*, 341–364. https://doi.org/10.1007/s10035-010-0230-7
Ericson, C. (2005). *Real-Time Collision Detection* (pp. 413–426). San Diego, CA: Morgan Kaufmann/Elsevier.
Feltham, D. L. (2005). Granular flow in the marginal ice zone. *Philosophical Transactions: Mathematical, Physical and Engineering Sciences*, *363*(1832), 1677–1700. https://doi.org/10.1098/rsta.2005.1601
Feltham, D. L. (2008). Sea ice rheology. *Annual Review of Fluid Mechanics*, *40*(1), 91–112. https://doi.org/10.1146/annurev.fluid.40.111406.102151
Flato, G. M., & Hibler, W. D. (1995). Ridging and strength in modeling the thickness distribution of Arctic sea ice. *Journal of Geophysical Research*, *100*(C9), 18611. https://doi.org/10.1029/95JC02091
Forterre, Y., & Pouliquen, O. (2008). Flows of dense granular media. *Annual Review of Fluid Mechanics*, *40*(1), 1–24. https://doi.org/10.1146/annurev.fluid.40.111406.102142
Fortt, A. L., & Schulson, E. M. (2007). The resistance to sliding along Coulombic shear faults in ice. *Acta Materialia*, *55*(7), 2253–2264. https://doi.org/10.1016/j.actamat.2006.11.022
Fortt, A. L., & Schulson, E. M. (2009). Velocity-dependent friction on Coulombic shear faults in ice. *Acta Materialia*, *57*(15), 4382–4390. https://doi.org/10.1016/j.actamat.2009.06.001
GDR-MiDi (2004). On dense granular flows. *European Physical Journal E: Soft Matter*, *14*, 341–365. https://doi.org/10.1140/epje/i2003-10153-0
Girard, L., Bouillon, S., Weiss, J., Amitrano, D., Fichefet, T., & Legat, V. (2011). A new modeling framework for sea-ice mechanics based on elasto-brittle rheology. *Annals of Glaciology*, *52*(57), 123–132. https://doi.org/10.3189/172756411795931499
Girard, L., Weiss, J., Molines, J. M., Barnier, B., & Bouillon, S. (2009). Evaluation of high-resolution sea ice models on the basis of statistical and scaling properties of Arctic sea ice drift and deformation. *Journal of Geophysical Research*, *114*, C08015. https://doi.org/10.1029/2008JC005182
Gladstone, R. M., Bigg, G. R., & Nicholls, K. W. (2001). Iceberg trajectory modeling and meltwater injection in the Southern Ocean. *Journal of Geophysical Research*, *106*(C9), 19,903–19,915. https://doi.org/10.1029/2000JC000347
Gnanadesikan, A., Dixon, K. W., Griffies, S. M., Balaji, V., Barreiro, M., Beesley, J. A., et al. (2006). GFDL's CM2 global coupled climate models. part II: The baseline ocean simulation. *Journal of Climate*, *19*(5), 675–697. https://doi.org/10.1175/jcli3630.1
Griffies, S. M., Gnanadesikan, A., Dixon, K. W., Dunne, J. P., Gerdes, R., Harrison, M. J., et al. (2005). Formulation of an ocean model for global climate simulations. *Ocean Science*, *1*(1), 45–79. https://doi.org/10.5194/os-1-45-2005
Gutfraind, R., & Savage, S. B. (1997a). Marginal ice zone rheology: Comparison of results from continuum-plastic models and discrete-particle simulations. *Journal of Geophysical Research: Oceans*, *102*(C6), 12,647–12,661. https://doi.org/10.1029/97JC00124
Gutfraind, R., & Savage, S. B. (1997b). Smoothed particle hydrodynamics for the simulation of broken-ice fields: Mohr-Coulomb-type rheology and frictional boundary conditions. *Journal of Computational Physics*, *134*(2), 203–215. https://doi.org/10.1006/jcph.1997.5681
Gutfraind, R., & Savage, S. B. (1998). Flow of fractured ice through wedge-shaped channels: Smoothed particle hydrodynamics and discrete-element simulations. *Mechanics of Materials*, *29*(1), 1–17. https://doi.org/10.1016/s0167-6636(97)00072-0
Henann, D. L., & Kamrin, K. (2013). A predictive, size-dependent continuum model for dense granular flows. *Proceedings of the National Academy of Sciences of the United States of America*, *110*(17), 6730–6735. https://doi.org/10.1073/pnas.1219153110
Herman, A. (2010). Sea-ice floe-size distribution in the context of spontaneous scaling emergence in stochastic systems. *Physical Review E*, *81*(6), 066123. https://doi.org/10.1103/physreve.81.066123

Herman, A. (2013). Shear-jamming in two-dimensional granular materials with power-law grain-size distribution. *Entropy*, *15*(11), 4802–4821. https://doi.org/10.3390/e15114802
Herman, A. (2016). Discrete-element bonded-particle sea ice model DESIgn, version 1.3a—Model description and implementation. *Geoscientific Model Development*, *9*(3), 1219–1241. https://doi.org/10.5194/gmd-9-1219-2016
Hibler, W. D. (1979). A dynamic thermodynamic sea ice model. *Journal of Physical Oceanography*, *9*(4), 815–846. https://doi.org/10.1175/1520-0485(1979)009<0815:adtsim>2.0.co;2
Hibler, W. D. (1980). Modeling a variable thickness sea ice cover. *Monthly Weather Review*, *108*(12), 1943–1973. https://doi.org/10.1175/1520-0493(1980)108<1943:mavtsi>2.0.co;2
Hopkins, M. A. (1996). On the mesoscale interaction of lead ice and floes. *Journal of Geophysical Research: Oceans*, *101*(C8), 18,315–18,326. https://doi.org/10.1029/96JC01689
Hopkins, M. A. (2004). A discrete element Lagrangian sea ice model. *Engineering and Computing*, *21*(2/3/4), 409–421. https://doi.org/10.1108/02644400410519857
Hopkins, M. A., Hibler, W. D., & Flato, G. M. (1991). On the numerical simulation of the sea ice ridging process. *Journal of Geophysical Research*, *96*(C3), 4809. https://doi.org/10.1029/90JC02375
Hopkins, M. A., & Thorndike, A. S. (2006). Floe formation in arctic sea ice. *Journal of Geophysical Research*, *111*, C11S23. https://doi.org/10.1029/2005JC003352
Horvat, C., & Tziperman, E. (2015). A prognostic model of the sea-ice floe size and thickness distribution. *Cryosphere*, *9*, 2119–2134. https://doi.org/10.5194/tc-9-2119-2015
Hunke, E. C., & Dukowicz, J. K. (1997). An elastic-viscous-plastic model for sea ice dynamics. *Journal of Physical Oceanography*, *27*(9), 1849–1867. https://doi.org/10.1175/1520-0485(1997)027<1849:aevpmf>2.0.co;2
Jop, P., Forterre, Y., & Pouliquen, O. (2006). A constitutive law for dense granular flows. *Nature*, *441*(7094), 727–730. https://doi.org/10.1038/nature04801
Kamrin, K., & Koval, G. (2014). Effect of particle surface friction on nonlocal constitutive behavior of flowing granular media. *Computational Particle Mechanics*, *1*(2), 169–176. https://doi.org/10.1007/s40571-014-0018-3
Kruggel-Emden, H., Sturm, M., Wirtz, S., & Scherer, V. (2008). Selection of an appropriate time integration scheme for the discrete element method (DEM). *Computers and Chemical Engineering*, *32*(10), 2263–2279.
Kwok, R., Pedersen, L. T., Gudmandsen, P., & Pang, S. S. (2010). Large sea ice outflow into the Nares Strait in 2007. *Geophysical Research Letters*, *37*(3). https://doi.org/10.1029/2009GL041872
Li, B., Li, H., Liu, Y., Wang, A., & Ji, S. (2014). A modified discrete element model for sea ice dynamics. *Acta Oceanologica Sinica*, *33*(1), 56–63. https://doi.org/10.1007/s13131-014-0428-3
Lindsay, R. W., & Stern, H. L. (2004). A new Lagrangian model of Arctic sea ice. *Journal of Physical Oceanography*, *34*(1), 272–283. https://doi.org/10.1175/1520-0485(2004)034<0272:anlmoa>2.0.co;2
Lipscomb, W. H., Hunke, E. C., Maslowski, W., & Jakacki, J. (2007). Ridging, strength, and stability in high-resolution sea ice models. *Journal of Geophysical Research*, *112*, C03S91. https://doi.org/10.1029/2005JC003355
Luding, S. (2008). Introduction to discrete element methods: Basic of contact force models and how to perform the micro-macro transition to continuum theory. *European Journal of Environmental and Civil Engineering*, *12*(7–8), 785–826.
Mair, K., Frye, K. M., & Marone, C. (2002). Influence of grain characteristics on the friction of granular shear zones. *Journal of Geophysical Research*, *107*, 2219.
Martin, T., & Adcroft, A. (2010). Parameterizing the fresh-water flux from land ice to ocean with interactive icebergs in a coupled climate model. *Ocean Modelling*, *34*(3–4), 111–124. https://doi.org/10.1016/j.ocemod.2010.05.001
Menge, J. A. R., & Jones, K. F. (1993). The tensile strength of first-year sea ice. *Journal of Glaciology*, *39*(133), 609–618. https://doi.org/10.1017/s0022143000016506
Mitchell, J. K., & Soga, K. (2005). *Fundamentals of Soil Behavior*. New York: Wiley.
Monaghan, J. J. (2012). Smoothed particle hydrodynamics and its diverse applications. *Annual Review of Fluid Mechanics*, *44*(1), 323–346. https://doi.org/10.1146/annurev-fluid-120710-101220
Morgan, J. K. (1999). Numerical simulations of granular shear zones using the distinct element method 2. Effects of particle size distribution and interparticle friction on mechanical behavior. *Journal of Geophysical Research*, *104*(B2), 2721–2732.
Morgan, J. K. (2015). Effects of cohesion on the structural and mechanical evolution of fold and thrust belts and contractional wedges: Discrete element simulations. *Journal of Geophysical Research: Solid Earth*, *120*, 3870–3896. https://doi.org/10.1002/2014jb011455
Nakayama, Y., & Boucher, R. F. (1998). Introduction to fluid mechanics. Oxford, MA: Butterworth-Heinemann. https://doi.org/10.1016/b978-034067649-3/50003-8
Nedderman, R. M. (1992). *Statics and Kinematics of Granular Materials*. Cambridge: Cambridge University Press.
Obermayr, M., Dressler, K., Vrettos, C., & Eberhard, P. (2013). A bonded-particle model for cemented sand. *Computers and Geotechnics*, *49*, 299–313. https://doi.org/10.1016/j.compgeo.2012.09.001
Peters, I. R., Amundson, J. M., Cassotto, R., Fahnestock, M., Darnell, K. N., Truffer, M., & Zhang, W. W. (2015). Dynamic jamming of iceberg-choked fjords. *Geophysical Research Letters*, *42*, 1122–1129. https://doi.org/10.1002/2014GL062715
Petrovic, J. J. (2003). Review: Mechanical properties of ice and snow. *Journal of of Materials Science*, *38*(1), 1–6.
Potyondy, D. O., & Cundall, P. A. (2004). A bonded-particle model for rock. *International Journal of Rock Mechanics and Mining Sciences*, *41*(8), 1329–1364.
Radjaï, F., & Dubois, F. (2011). *Discrete-Element Modeling of Granular Materials* (pp. 425). London, UK: Wiley-Iste.
Rallabandi, B., Zheng, Z., Winton, M., & Stone, H. A. (2017a). Wind-driven formation of ice bridges in straits. *Physical Review Letters*, *118*, 128701. https://doi.org/10.1103/physrevlett.118.128701
Rallabandi, B., Zheng, Z., Winton, M., & Stone, H. A. (2017b). Formation of sea ice bridges in narrow straits in response to wind and water stresses. *Journal of Geophysical Research: Oceans*, *122*, 5588–5610. https://doi.org/10.1002/2017jc012822
Rampal, P., Bouillon, S., Ólason, E., & Morlighem, M. (2016). NeXtSIM: A new Lagrangian sea ice model. *Cryosphere*, *10*(3), 1055–1073. https://doi.org/10.5194/tc-10-1055-2016
Reynolds, O. (1885). On the dilatancy of media composed of rigid particles in contact. *Philosophical Magazine*, *20*(5), 46.
Robel, A. A. (2017). Thinning sea ice weakens buttressing force of iceberg mélange and promotes calving. *Nature Communications*, *8*, 14596. https://doi.org/10.1038/ncomms14596
Rothrock, D. A. (1975). The energetics of the plastic deformation of pack ice by ridging. *Journal of Geophysical Research*, *80*(33), 4514–4519. https://doi.org/10.1029/JC080i033p04514
Rudnicki, J. W., & Rice, J. R. (1975). Conditions for the localization of deformation in pressure-sensitive dilatant materials. *Journal of the Mechanics and Physics of Solids*, *23*(6), 371–394.

Samelson, R. M., Agnew, T., Melling, H., & Münchow, A. (2006). Evidence for atmospheric control of sea-ice motion through Nares Strait. *Geophysical Research Letters*, *33*, L02506. https://doi.org/10.1029/2005GL025016

Schulson, E. M. (1999). The structure and mechanical behavior of ice. *Journal of the Minerals Metals and Materials Society*, *51*(2), 21–27. https://doi.org/10.1007/s11837-999-0206-4

Schulson, E. M. (2001). Brittle failure of ice. *Engineering Fracture Mechanics*, *68*(17–18), 1839–1887. https://doi.org/10.1016/s0013-7944(01)00037-6

Schulson, E. M., & Fortt, A. L. (2012). Friction of ice on ice. *Journal of Geophysical Research*, *117*, B12204. https://doi.org/10.1029/2012JB009219

Schulson, E., Fortt, A., Iliescu, D., & Renshaw, C. (2006). On the role of frictional sliding in the compressive fracture of ice and granite: Terminal vs. post-terminal failure. *Acta Materialia*, *54*(15), 3923–3932. https://doi.org/10.1016/j.actamat.2006.04.024

Steer, A., Worby, A., & Heil, P. (2008). Observed changes in sea-ice floe size distribution during early summer in the western Weddell Sea. *Deep Sea Research Part II: Topical Studies in Oceanography*, *55*(8–9), 933–942. https://doi.org/10.1016/j.dsr2.2007.12.016

Tang, J., Sagdiphour, S., & Behringer, R. P. (2009). Jamming and flow in 2D hoppers. In *Proceedings of the 6th International Conference on Micromechanics of Granular Media. AIP Conference Proceedings* (Vol. 1145, pp. 515–518). Golden, CO: AIP Conference Proceedings. https://doi.org/10.1063/1.3179975

Terzaghi, K., Peck, R. B., & Mesri, G. (1996). *Soil Mechanics in Engineering Practice* (3rd ed.). New York: John Wiley.

Thomas, C. C., & Durian, D. J. (2015). Fraction of clogging configurations sampled by granular hopper flow. *Physical Review Letters*, *114*, 178001. https://doi.org/10.1103/physrevlett.114.178001

Thorndike, A. S., Rothrock, D. A., Maykut, G. A., & Colony, R. (1975). The thickness distribution of sea ice. *Journal of Geophysical Research*, *80*(33), 4501–4513. https://doi.org/10.1029/JC080i033p04501

To, K., Lai, P.-Y., & Pak, H. K. (2001). Jamming of granular flow in a two-dimensional hopper. *Physical Review Letters*, *86*(1), 71–74. https://doi.org/10.1103/physrevlett.86.71

Tremblay, L.-B., & Mysak, L. A. (1997). Modeling sea ice as a granular material, including the dilatancy effect. *Journal of Physical Oceanography*, *27*(11), 2342–2360. https://doi.org/10.1175/1520-0485(1997)027<2342:msiaag>2.0.co;2

Weiss, J., & Schulson, E. M. (2009). Coulombic faulting from the grain scale to the geophysical scale: Lessons from ice. *Journal of Physics D: Applied Physics*, *42*(21), 214017. https://doi.org/10.1088/0022-3727/42/21/214017

Weiss, J., Schulson, E. M., & Stern, H. L. (2007). Sea ice rheology from in-situ, satellite and laboratory observations: Fracture and friction. *Earth and Planetary Science Letters*, *255*(1–2), 1–8. https://doi.org/10.1016/j.epsl.2006.11.033

Wilchinsky, A. V., & Feltham, D. L. (2006). Modelling the rheology of sea ice as a collection of diamond-shaped floes. *Journal of Non-Newtonian Fluid Mechanics*, *138*(1), 22–32. https://doi.org/10.1016/j.jnnfm.2006.05.001

Wilchinsky, A. V., Feltham, D. L., & Hopkins, M. A. (2010). Effect of shear rupture on aggregate scale formation in sea ice. *Journal of Geophysical Research*, *115*, C10002. https://doi.org/10.1029/2009JC006043

Wilchinsky, A. V., Feltham, D. L., & Hopkins, M. A. (2011). Modelling the reorientation of sea-ice faults as the wind changes direction. *Annals of Glaciology*, *52*(57), 83–90. https://doi.org/10.3189/172756411795931831

Zuriguel, I. (2014). Invited review: Clogging of granular materials in bottlenecks. *Papers in Physics*, *6*, 060014. https://doi.org/10.4279/pip.060014